ORIGINAL ARTICLE

Diffusion tensor based motion correction enables multi-parametric imaging of human placenta microstructures

Zhexian Sun[1,2], Wenjie Wu[1,2], Peinan Zhao[2], Anthony Odibo[2], Qing Wang[3], Yong Wang[1,2,3,4]

[1]Department of Biomedical Engineering, Washington University in St. Louis School of Medicine, St. Louis 63130, MO, USA;
[2]Department of Obstetrics and Gynecology, Washington University in St. Louis School of Medicine, St. Louis 63130, MO, USA;
[3]Mallinckrodt Institute of Radiology, Washington University in St. Louis School of Medicine, St. Louis 63110, MO, USA;
[4]Department of Electrical & Systems Engineering, Washington University in St. Louis, St. Louis 63130, MO, USA

Abstract

Background: Non-invasive *in vivo* diffusion-weighted magnetic resonance imaging (DWI) of the human placenta allows safe imaging and accurate characterization of the microstructure of the placenta during pregnancy. However, misalignment of different diffusion-weighted images caused by the maternal and fetal motion severely compromised the accuracy of diffusion magnetic resonance imaging (MRI) quantification. In this study, we proposed a diffusion tensor-based registration method customized to correct the image misalignment in DWI and enhance the multi-parametric imaging of human placenta microstructures. **Method:** We developed a novel registration method based on the diffusion tensor imaging (DTI) model and Fourier-approximated Lie Algebras for Shooting (FLASHC). We extensively tested and validated our method using simulated DWI images, which were contaminated by motion and deformation of the placenta. DWI of the entire uterus was acquired in 86 different directions with bmax = 2000 s/mm². Our method is quantitatively evaluated using the continuous dice coefficient (cDC) and fitting residue from DTI and diffusion basis spectrum imaging (DBSI). Our method enables the application of advanced and complicated diffusion analysis models and detailed cotyledon-wise quantification of human placenta microstructural features. **Result:** The proposed method was proven efficient in registering simulated DWI deformed by motion, with increase mean cDC (from 0.78 to 0.93) and decrease mean fitting residue (DTI from 10.95% to 9.01%, DBSI from 8.01% to 3.07%). Similar improvements were found in registering DWI from clinical patients (cDC from 0.79 to 0.86 , DTI from 34.7 to 28.2%, DBSI from 6.5 to 2.8%.). Also, DBSI derived maps showed reasonable pattern after registration. After cotyledon-wise segmentation, region regional increased cellularity ratio was found in one patient with placental cyst and infarction. **Conclusion:** The proposed registration method provides a robust framework for motion correction in diffusion-weighted MR images and enabled the detailed and accurate quantification of human placenta microstructures.

Key words: placental diffusion magnetic resonance imaging, image registration, diffusion basis spectrum imaging, cotyledon-wise analysis

INTRODUCTION

The human placenta is an important but least understood organ.[1] A proper functional placenta is necessary for fetal well-being since it works as a source of oxygen and nutrients for the fetus while also eliminating carbon dioxide and other waste products.[2] A better understanding of the placental structure and function, as well as its connection

with fetal development would benefit women, children and families enormously.[3] To assess the placental condition in a non-invasive fashion, applications from a variety of medical imaging modalities, including ultrasound, magnetic resonance imaging (MRI), and optical imaging, have been applied.

MRI is a radiation-free imaging modality that may produce high-resolution images of any region of the human body.[4] MRI include a variety of types including T1,T2,T2* diffusion weighted MRI (DWI), MR angiography (MRA), conducted by different MRI sequences and scan parameters to reveal different local tissue properties.[5]

DWI is a non-invasive *in vivo* imaging technique in Obstetrics. Additionally, DWI is a straightforward structural imaging technique to implement in the placenta because it is routinely utilized in other organ and does not require any exogenous contrast agent.[6] The DWI contrast is determined by the microscopic mobility of water molecule.[7] Microstructure (*e.g.* the cell membrane) inhibits water molecule diffusivity, which could be valuated and quantified using diffusion measurements such as apparent diffusion coefficient (ADC). Deviation in diffusion measurements can further reflect the local pathological alteration.

As a commonly used DWI model in clinic, Diffusion Tensor Imaging (DTI) was employed to compare the placental ADC deviation in Intrauterine growth restriction (IUGR) cases by Görkem *et al.*[8] To investigate the placental perfusion, Siauve *et al.*[9] employed Intravoxel incoherent motion imaging (IVIM) to predict intrauterine growth retardation (SGA). A more advanced multi-compartment DWI analysis model was used to separate the fetal and maternal blood by Aughwane *et al.*[10]

However, DWI typically take a long scan time, which raises the issue of misalignment caused by maternal and fetal motion. Image registration is a critical component of pre-processing since it corrects motion deformation. The significance of analysis is heavily dependent on motion correction, as the majority of diffusion analysis tools treat

each voxel independently and assume the absolute voxel-wise alignment as pre-condition. Hence, a proper geometric transformation is needed to cancel the deformation.

In this paper, we proposed a novel registration pipeline specifically developed for placental DWI registration. The pipeline employed a simulated target image as a reference for voxel-intensity-based registration to counter the distraction from contrast differences. With better aligned DWI data, we further applied an advanced diffusion analysis model, diffusion basis spectrum imaging (DBSI) and detailed cotyledon-wise segmentation on one patient with normal pregnancy and one patient with placental cyst and infarction.

MATERIAL AND METHOD

DWI data Acquisition
This study was approved by the Washington University in St. Louis Institutional Review Board (IRB ID: 201707152). DWI was performed on a 3T Siemens Vida scanner (Siemens, Erlangen, Germany). Two patients with singleton pregnancy underwent MRI. The study was explained to them and the informed consent document was signed. Information on patients' medical history and labor outcome can be found in Table 1.

DWI imaging of the entire uterus was acquired with a 2D EPI sequence under different weightings with bmax = 2000 s/mm². A total of 86 frames (b-table was specially designed for DBSI, 86 different directions and 30 different b-values) was acquired. Other acquisition parameters were: 12.8 s repetition time; 62 msec echo time; 3 mm slices thickness; 3×3 mm² in-plane resolution.

Manual segmentation
Manual segmentation of the placenta was performed by experienced OB&GYN radiologists. For one patient, segmentations were performed on 13 frames to compute the continuous dice coefficient (cDC) to quantify the following improvement. All segmentations are performed

Table 1: Demographic information.

Characteristics	Pt 1	Pt 2
Age, y	36	34
BMI (before pregnancy / at delivery)	25.71 / 30.59	23.24 / 31.95
Medical History	No documented medical history	1. PE with severe features 2. anaplastic ependymoma 3. epilepsy at 37 weeks GA
GA at Delivery	39w0d	37w0d
Placenta Pathology	No histopathological abnormality	1. incidental septal cyst (2cm in greatest dimension) 2. infarct (1.5cm in greatest dimension)
Fetal Weight/Length/Head circumference	3910g / 52.0cm / 35.5cm	3265g / 50.5cm / 34.5cm
Labor outcome	Live female neonate	Live male neonate

Pt: patient; BMI: body mass index; GA: gestational age; PE: preeclampsia.

in Medical Imaging Interaction Toolkit (MITK).[11]

Image registration

Prior to registration, Marchenko-Pastur (MP) denoising and bias correction was conducted to each frame.[12]

A diffusion tensor map was computed using a subset of frames with minimal misalignments. Simulated reference frames were obtained by computing voxel-wise diffusion decay using the equation below

$$S = S_0 * \exp(-\|\vec{b_k}\| v^T D v)$$

Where S_0 is the voxel intensity in the T2 weighted image (T2WI) with zero diffusion weighting (B_0). $\vec{b_k}$ is the kth diffusion weighting gradient, v is a unit vector has the same direction as b_k. D is voxel-wise diffusion tensor.

FLASHC was utilized to register each DWI to the corresponding simulated reference image.

FLASHC is a C++ application of the fast Large deformation diffeomorphic metric mapping (LDDMM) algorithm that minimizes the following target function in Fourier space.

$$\min \left(\int_0^1 \|v_t\|_V^2 dt + \|I_0 \circ \phi_1^{-1} - I_1\|_{L^2}^2 \right)$$

where the first term is an appropriate Sobolev norm on the initial velocity field of the transform matrix ϕ_1^{-1}, the second term enforces matching of the image with L2-norm.

I_0 and I_1 are the source and target image respectively. And $I_0 \circ \phi_1^{-1}$ derives the deformed source image, which is the output of registration process.

Registration evaluation and validation

The cDC[13] was employed to quantitatively evaluate the performance of registration. Segmentations from both the source and target image were required to compute cDC. We expect an increase in the cDC score following the application registration procedure to reflect the improvement of alignment.

We validated the performance of our registration pipeline by doing a test registration on the DWI with simulated motion misalignment. Nonetheless, cDC score will be computed prior to and following registration to quantify the image alignment.

Another metric to quantify the image alignment is the fitting residue R, defined by the following equations:

$$R_{DTI} = abs(f - \exp(-b * D))/f$$
$$R_{DBSI} = abs(f - S * \lambda)/f$$

Where f is the measured signal, b is the b-value, D is the computed diffusion tensor in DTI, S is the computed

spectrum in DBSI, λ is the designed basis in DBSI.

Diffusion tensor imaging and diffusion basis spectrum imaging

DTI was conducted to reconstruct voxel-wise diffusion tensors by least square fitting. Apparent diffusion coefficient (ADC) and fractional anisotropy (FA) maps are presented based on the computed diffusion tensor.

DBSI was used to image microstructural composition.[14] While the full spectrum includes both isotropic and anisotropic components, we focus on the isotropic parts in this study. Further, we sum up the spectrum in different ranges to derive five parameters: (1) Cellularity ratio, which includes isotropic tensors with ADC less than 0.9×10^{-3} mm^2/s; (2) Hindered diffusion ratio, which has an ADC between 0.9×10^{-3} mm^2/s and 2.5×10^{-3} mm^2/s; (3) Free diffusion ratio, which has an ADC between 2.5×10^{-3} mm^2/s and 10×10^{-3} mm^2/s; (4) Perfusion ratio, which has an ADC greater than 10×10^{-3} mm^2/s; (5) Total isotropic ratio, which is the summation of the ratios of parameters (1) to (4).

Cotyledon-wise segmentation

To obtain the segmentation of each cotyledon in placenta, we asked experienced radiologist to place seeds inside each cotyledon. The area of each cotyledon is then defined using a region growth method. The region's growth is complete when the volume stops expanding or reaches a threshold.

RESULTS

Simulated DWI data

Based on real patients' tensor map (Figure 1A) and the b-table used in clinical scan, we generated simulated full DWI data (Figure 1B). Simulated transform matrices (Figure 1C) were applied on DWI images to produce deformed DWI images (Figure 1D). The transform matrices were continuous spatially and temporally to mimic the realistic patient motion. Then, we applied our registration pipeline (Figure 1E–G) and evaluated the improvement (Figure 1H).

Evaluation of placenta DWI pipeline using simulated DWI data with motion

Two types of motion were modelled based on real MR image (Figure 2A) in the simulation: (1) slow motion, which causes gradual misalignments lasting ten frames (Figure 2B, red arrow). (2) fast motion, which causes abrupt misalignments between two adjacent frames (Figure 2B, blue arrow).

To visualize the alignment, a 128 × 6 segment of each volume in the same location was extracted and spliced along the time axis. After registration, we observed a significant improvement in image alignment (Figure 2C).

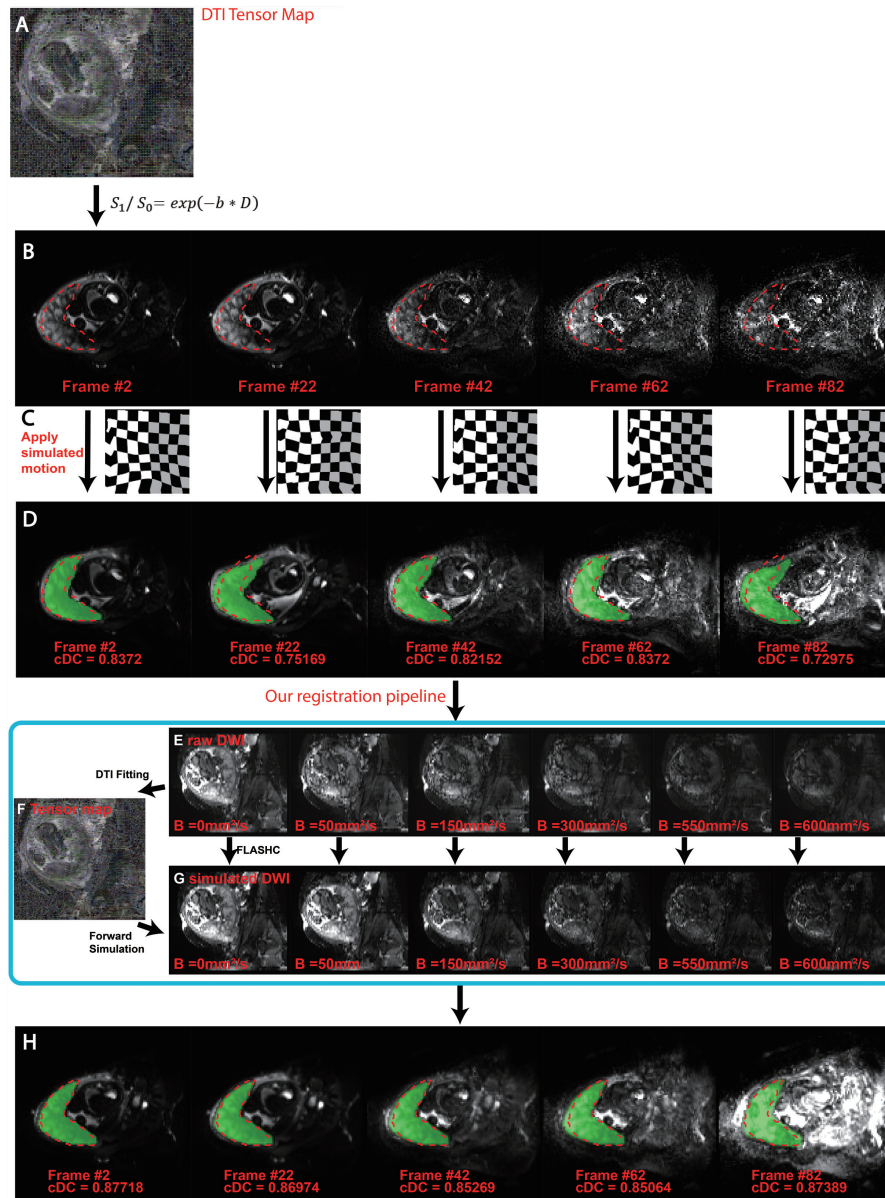The simulated motion resulted in a dramatic drop in the

Figure 1. Flowchart of validating registration pipeline using simulated DWI with motion. (A): First, the simulation started from a tensor map. We selected a tensor map computed from Pt 1's DWI data. (B): Secondly, we generate the full DWI data based on the tensor map and the b-table. All frames shared the same placenta segmentation since they are from one tensor map (red contour). Several exemplary frames were presented. (C): The transform matrix is randomly generated and subject to the spatial and temporal continuity to mimic realistic motion. (D): Thirdly, we apply the transform matrix to simulate the motion deformation for each DWI frame and the placenta segmentation (green area: deformed ROI, red contour: original ROI). cDC scores between the segmentation before and after deformation were presented. (E): Next, we used our registration pipeline to process the simulate DWI data with motion, (F) Tensor map. A subset with highest mutual information score to the b0 image was extracted and used to compute the voxel-wise diffusion tensor.(G) Simulated DWI. For each diffusion weighted image, a reference image was created based on the tensor map and b-table. In our pipeline, we register the original DWI image to the corresponding simulated reference image. (H) The output registered DWI. Pt: patient; DTI: diffusion tensor imaging; DWI: diffusion-weighted magnetic resonance imaging; cDC: continuous dice coefficient; ROI: region-of-interest.
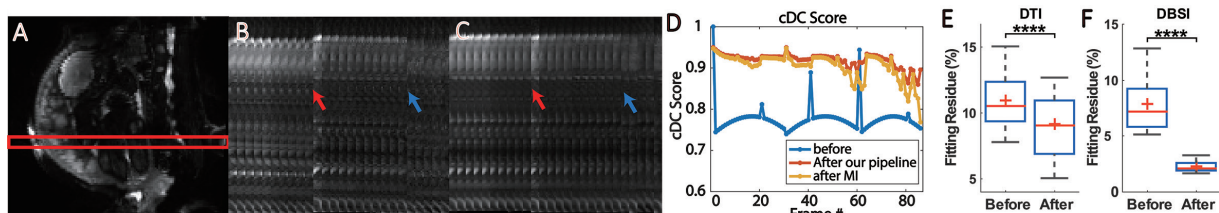

Figure 2. Test registration in simulated DWI. (A): b0 in simulated DWI data, red contour denotes the location of 128×6 segment. (B): 1st–20th frames from the unregistered simulated DWI; (C): 1st–20th frames from the registered simulated DWI. Two remarkable motion misalignments before and after registration were marked in blue and red arrows. (D): cDC score from three different methods; (E): DTI fitting residual before and after registration. (F): DBSI fitting residual before and after registration. DTI: diffusion tensor imaging; DWI: diffusion-weighted magnetic resonance imaging; DBSI: diffusion basis spectrum imaging; cDC: continuous dice coefficient. ****$p < 0.001$.
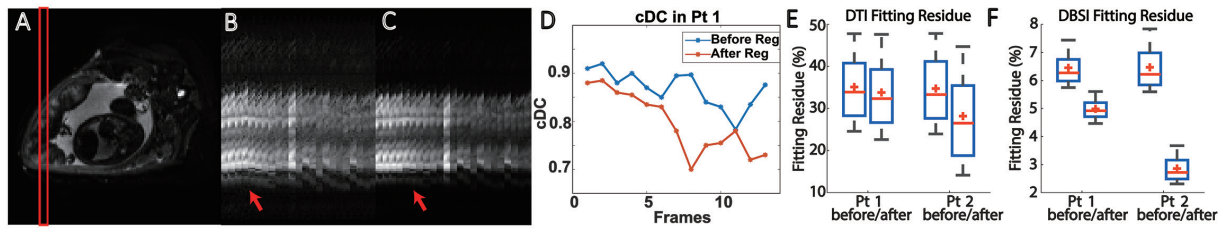
Figure 3. Registration pipeline correct the image misalignment in DWI images. (A): b0 in simulated DWI data, red contour denotes the location of 128×6 segment; (B): 1st–20th frames from the unregistered clincal DWI; (C) 1st–20th frames from the registered clincal DWI. Red arrow shows an exemplary misalignment fixed by registration. (D): cDC score from 1st–13th frame before and after registration; (E): DTI fitting residual decreased after registration in both patients. (F): DBSI fitting residual decreased after registration in both patients. DWI: diffusion-weighted magnetic resonance imaging; DTI: diffusion tensor imaging; DBSI: diffusion basis spectrum imaging; cDC: continuous dice coefficient.
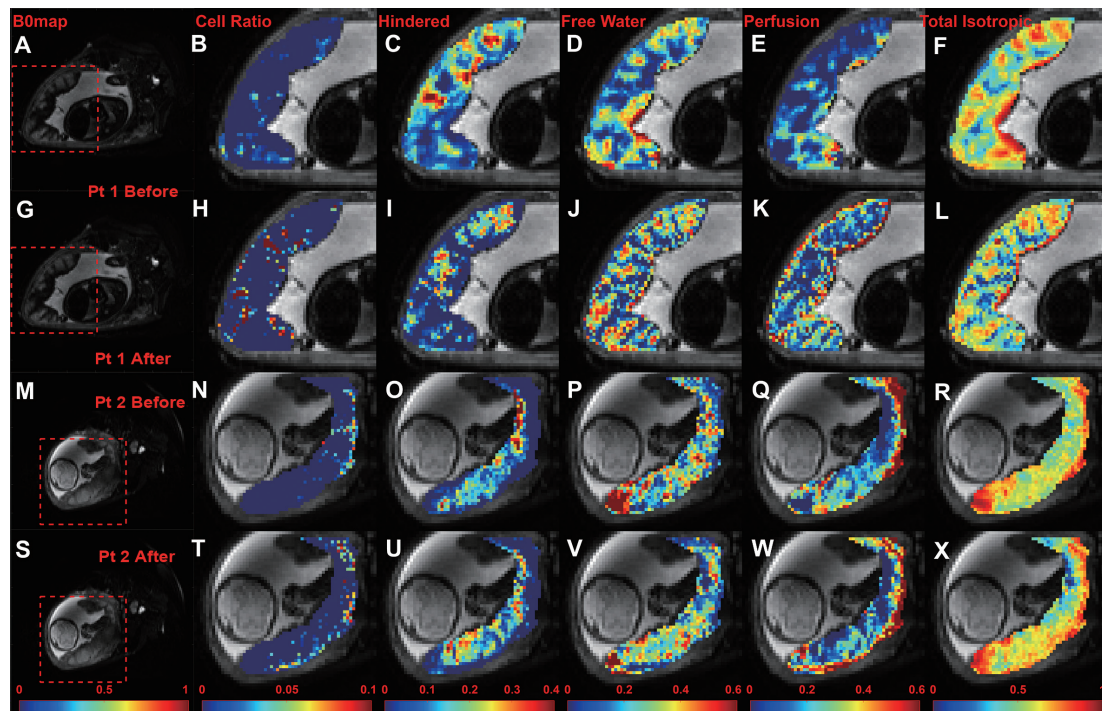

Figure 4. Full DBSI results before and after registration, from two patients. First row (A–F): b0 map, cellularity ratio, hindered diffusion ratio, free diffusion ratio, perfusion ratio and total ratio of isotropic components from Pt 1 before registration. Second row (G–L): Pt 1 results after registration. Third row (M–R): Pt 2 results before registration. Fourth row (S-X): Pt 2 results after registration. Pt 1: a patient with pregnancy with no detected abnormality, MRI at 35 weeks GA; Pt 2: a patient diagnosed with incidental septal cyst and infarct, MRI at 33 weeks GA. MRI: magnetic resonance imaging; GA: gestational age.
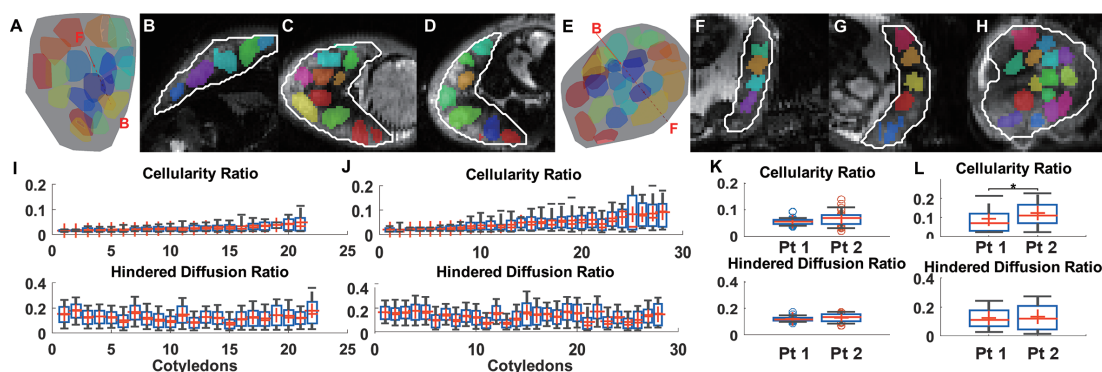

Figure 5. Cotyledon-wise placental analysis. (A): 3d view of the segmentations of entire placenta and 22 segmented cotyledons. The position of umbilical cord was marked by the red bar. Basal plate side marked by B, and fetal side marked by F; (B–D): placenta segmentation and cotyledon segmentations in sagittal, coronal, axial view. Placenta region was marked by white lines, color-encoded region were the segmented cotyledons. (E): The 3d view of segmentations in Pt 2, 28 cotyledons in total. (F–H): Placenta segmentation and cotyledon segmentations in sagittal, coronal, axial view. (I): cotyledon-wise cellularity ratio and hindered diffusion ratio from Pt 1. (J): cotyledon-wise cellularity ratio and hindered diffusion ratio from Pt 2. (K): Boxplot of two selected cotyledon; (L): Boxplot of mean value in each cotyledon from Pt 1 and Pt 2. Statistic exam conducted by Wilcoxon ranksum exam. *$p < 0.05$. Pt: patient.

cDC score (Figure 2D, cDC = 0.78 ± 0.092). We evaluated image registration using two methods: (1) our registration pipeline and (2) a registration tool that uses the mutual information metric (Figure 2D). While both registration method improved the cDC score, our method showed better performance (cDC = 0.933 ± 0.011) than directly register DWI by mutual information-based methods (cDC = 0.898 ± 0.047), especially in high b-value DWI images. We repeated the full workflow showed in Figure 1 using clinical DWI data from 20 patients and compared the fitting residues.

After registration, the fitting residues from both DTI and DBSI reduce significantly (Figure 2E–F DTI fitting residues reduce from 10.95% ± 2.74% to 9.01% ± 2.77%, DBSI fitting residues reduce from 8.01% ± 2.51% to 3.07% ± 0.84%).

Evaluation of placenta DWI pipeline using clinical DWI data

The same analysis was performed on the clinical data. (Figure 3A, diffusion tensor map from one patient). Deformation in the raw DWI was better aligned after registration (Figure 3B–C, red arrow). The registration pipeline restores not only the spatial alignment of the placenta boundary, but also the interior texture representing the intra-placental structure and cotyledon units.

To quantify the registration performance, we performed manual segmentation on from the first to 13th DWI images for the Patient 1. We observed an increase in cDC score following the registration. Except for the 11th frame, the rest of cDC scores are no less than 0.8 (Figure 3D). After registration, fitting residues from both DTI and DBSI reduce (Figure 3E–F In Patient 1: DTI fitting residues reduce from 35.1% ± 8.7% to 33.8% ± 9.5%, DBSI fitting residues reduce from 6.4% ± 0.7% to 5.0% ± 0.5%, In Patient 2: DTI fitting residues reduce from 34.7% ± 8.9% to 28.2% ±11.9%, DBSI fitting residues reduce from 6.5% ± 0.8% to 2.8% ± 0.5%).

Registered DWI data produce more convincing DBSI results

After registration, DBSI was employed to analyze the registered DWI images and extract the parameters describing sub-voxel information. Maps of cellularity ratio, hindered diffusion ratio, free diffusion ratio, perfusion ratio and total isotropic component ratio are presented in Figure 4.

In our theory: (1) cellularity represents immune cell infiltration (Figure 4B, H, N, and T); (2) hindered diffusion ratio represent the diffusion in matured terminal villa with rich membrane in healthy cases and local tissue edema in pathological cases(Figure 4C, I, O, and U); (3) free diffusion ratio represents less matured villa(Figure 4D, J, P, and V); (4): perfusion ratio represent fast blood flow in

the vessel (Figure 4E, K, Q, and W); (5): total isotropic component ratio (Figure 4F, L, R, and X) is the summation of (1) to (4).

We presented and compared the DBSI derived maps of the placentas before and after registration. After registration, patterns from all DBSI maps changed remarkably. We saw cellularity increase in both intensities and areas. And the cellularity is more evenly distributed in placenta. In Patient 1, the free diffusion ratio map reveals clearer pattern of cotyledons after registration. Also, we observed increased perfusion component near the basal plate, which is consistent with the physiology and previous publication.[15]

Cotyledon based image analysis

We used a semi-automatic method to segment the cotyledons in placenta. In Patient 1, 22 cotyledons were identified, the segmented area comprise 62% total placenta volume. In Patient 2, 28 cotyledons were identified, the segmented area comprise 57% total placenta volume (Figure 5A–H). We further study the voxel-wise value in each cotyledon as well as in the entire placenta. We found that Patient 2 showed larger variance in cotyledon-wise mean cellularity (Patient 1, 5.6% ± 1.2%; Patient 2, 7.0% ± 3.2%). In Patient 1, most of the cotyledon had a baseline mean cellularity ratio around 0.05. In Patient 2, three cotyledons showed abnormally mean high cellularity > 0.1. We further compared the cotyledon with highest cellularity from the two patients (Figure 5K), found significant different in cellularity ratio but not hindered diffusion ratio. We also presented the mean value in each cotyledon (Figure 5L), neither ratio showed significant differences.

DISCUSSION

In this paper we introduce a registration pipeline optimized for placental DWI based on FLASHC. FLASHC is a voxel-wise intensity based non-rigid registration algorithm. The algorithm search for voxel pairs in target and source image with similar voxel intensity. However, the optimization become hard to converge when the source and target image are from different contrast or modality.[16] DWI dataset has different contrast due to the changing diffusion weighting, hence, directly register all the frame to the first volume would not work with intensity-based method.[17] Both misalignment and contrast difference contribute the loss function, consequently the loss function did not solely represent image alignment. In the pipeline we built, we used forward simulated image as the target to minimize the contrast difference.

Quantitatively, the increase in cDC indicates a better alignment. Also in the figure, we found that our registration pipeline not only register the boundary of placenta, but also align the interior texture including cotyledon boundaries. We prefer cDC over DICE because the deformed segmentation mask might contain decimal, while the DICE

index is only able to take binary mask as input.

However, compare the registration result from DWI with simulated motion and clinical DWI from real patients, we found that the registration performance on the former often exceed the latter. Several contributing factors are:

(1) We only model the motion deformation in the simulated DWI. However, in the clinical DWI, other imaging artifacts,[18] data loss due to acquisition error,[19] and signal inhomogeneity due to coil[20] would affect the distract the registration.

(2) The actual motion in pregnant patient might not subject to spatial continuity: The motion of fetus can be independent to the motion of uterus wall and placenta. Registration becomes hard to converge, as FLASHC assumes the spatial continuity of transformation.

We wanted to firstly conduct sold image registration before applying more advanced diffusion analysis model. Without good image quality, the more complex model might amplify the artifacts instead of real signal. We applied DBSI on the registered DWI data, the computed parameter maps further revealed the altered immune response and placental circulation in Patient 2.

Given the remarkable heterogeneity, an average value of entire placenta is not appropriate to describe the placental condition. More detailed segmentations of subregions are in need. We used a semi-automatic region growth algorithm to segment regions of individual cotyledons, as we noticed there are visually appreciable cotyledon structures on T2WI, especially in the late pregnancy. The high signal region from blood rich intervillous spaces were divided by low signal region from placenta septa, such pattern was reported in previous studies on T2WI and T2* maps.[21-23] We set conservative stop criterion to prevent the region growth iteration from exceeding to its neighbor cotyledon. The semi-automatic segmentation method based on region grow method and consider only voxel intensity on the b0 map.

The cellularity ratio comes from immune cell infiltration.[13] There will be residue immune cell and baseline immune response even in the healthy placenta as the normal pregnancy undergoes pro-inflammatory during the third trimester.[24, 25] From the boxplot (Figure 5I and J), baseline immune response explains the low cell ratio in most of cotyledon in both Patient 1 and Patient 2. And the mean cellularity ratio from each cotyledon didn't show significant difference between two patients (Figure 5K). However, there was significant higher voxel-wised cellularity ratio in one cotyledon from Patient 2 (Figure 5L). This cotyledon is very like the foci of pathology, where on top of the baseline immune response, placental lesion brought additional

cellularity ratio, which induce more restricted diffusion, matches the reduced ADC reported in previous study.[26] Also, it indicated that the additional immune response from such cotyledon abnormality is local, not in all cotyledons.

There are both hindered diffusion ratio and free diffusion ratio in the cotyledon, the membrane structure in terminal villa hindered the diffusion in the IVS and cause reduced ADC. However, in less matured cotyledon or malfunction cotyledon, we anticipate there will be less hindered diffusion ratio and more free diffusion ratio due to the low density of terminal villa.[27] While the cotyledon-wise mean hindered diffusion ratio between two patients didn't show significant differences, those in Patient 2 show larger variance (Figure 5L), possibly suggesting the accelerated villous maturation as the compensatory change due to altered placental perfusion.[28]

A more regular pattern was seen on Patient 1's free diffusion ratio map (Figure 4J), which revealed the underlying separated cotyledon structure (high value indicates blood-rich intervillous space, low value area near the basal plate indicates placenta septa, low value area near the chorionic plates indicates villous tree [Supplementary Material]). On the contrary, the free diffusion ratio was possibly intervened by altered blood flow due to infarction and cyst in Patient 2 (Figure 4V).

The perfusion ratio in placenta mainly represents the fast blood flow in major vessels, including maternal vessel at the basal plate and fetal vessel at the chorionic plate.[29] In both patients, the high perfusion ratio areas are located in periphery of the placenta (Figure 4K and W). However, in Patient 1 both fetal and maternal side showed high perfusion (Figure 4K), such pattern well matched the distribution of these two parts of vessels and previous studies.[30-32] While in Patient 2 the perfusion near fetal side is weaker (Figure 4W). Similar results were reported in Doppler ultrasound study, where placental infarction induce increased uterine artery pulsatility index (PI) and reduced PI on the fetal side.[33, 34]

In the selected DBSI parameters, the cotyledon-wise mean value had a larger range (Figure 5I–L), indicating the cotyledon condition is less consistency compared to the healthy case. Moreover, while the pathological foci and additional cellularity is local and limited in few cotyledons, it tends to lead global affect and intervene the entire placenta circulation. Consequently, resulted in altered placental hinder diffusion, free diffusion and perfusion ratio.

Further, this technique would also elevate the connection between *ex-vivo* and *in-vivo* placental assessment. With the distribution of cotyledons denoted *in-vivo*, radiologists can retrieve the *ex-vivo* pathology findings, and pathologists can exam the tissue from the detected abnormal cotyledon specifically.

There are several limitations in this study. Two manual inputs are required for the proposed semi-automatic method: (1) A manual placenta segmentation is needed before the cotyledon-wise segmentation (2) Origins are needed as the seeds of region growing for detecting each cotyledon. Also, only two patients were included in this paper for demonstrating the feasibility of methodology. In the future, we need large sample volume to better validate the correlation between DBSI measurement and cotyledon/placental outcomes.

Supplementary Materials

Supplementary materials mentioned in this article are online available at the journal's official site only.

Ethics Approval and Consent to Participate

This study was approved by the Washington University in St. Louis Institutional Review Board (IRB ID: 201707152). The informed consent document was signed.

Source of Funding

Conflict of Interest

Yong Wang is an Editorial Board Member of the journal. The article was subject to the journal's standard procedures, with peer review handled independently of this member and his research group.

REFERENCES

1. Guttmacher AE, Maddox YT, Spong CY. The Human Placenta Project: placental structure, development, and function in real time. Placenta 2014;35:303–304.

2. Gude NM, Roberts CT, Kalionis B, King RG. Growth and function of the normal human placenta. Thromb Res 2004;114:397–407.

3. Garnica AD, Chan WY. The role of the placenta in fetal nutrition and growth. J Am Coll Nutr 1996;15:206–222.

4. Suetens P. Fundamentals of Medical Imaging. 2nd ed. Cambridge: Cambridge University Press, 2009.

5. Brown RW, Cheng YCN, Haacke EM, Thompson MR, Venkatesan R. Magnetic resonance imaging: physical principles and sequence design. 2nd ed. New Jersey : John Wiley & Sons, 2014.

6. Siauve N, Chalouhi GE, Deloison B, Alison M, Clement O, Ville Y, *et al.* Functional imaging of the human placenta with magnetic resonance. Am J Obstet Gynecol 2015;213:S103–S114.

7. Campbell JSW, Bruce Pike G. Diffusion Magnetic Resonance Imaging. In: Narayan R, editor. Encyclopedia of Biomedical Engineering. Oxford: Elsevier, 2019:505–518.

8. Görkem SB, Coşkun A, Eşlik M, Kütük MS, Öztürk A. Diffusion-weighted imaging of placenta in intrauterine growth restriction with worsening Doppler US findings. Diagn Interv Radiol 2019;25:280–284.

9. Siauve N, Hayot PH, Deloison B, Chalouhi GE, Alison M, Balvay D, *et al.* Assessment of human placental perfusion by intravoxel incoherent motion MR imaging. J Matern Fetal Neonatal Med 2019;32:293–300.

10. Aughwane R, Mufti N, Flouri D, Maksym K, Spencer R, Sokolska M, *et al.* Magnetic resonance imaging measurement of placental perfusion and oxygen saturation in early-onset fetal growth restriction. BJOG 2021;128:337–345.

11. Wolf I, Vetter M, Wegner I, Nolden M, Böttger T, Hastenteufel M, *et al.* The Medical Imaging Interaction Toolkit (MITK) – a toolkit facilitating the creation of interactive software by extending VTK and ITK. Proc SPIE 2004;5367:16–27.

12. Veraart J, Novikov DS, Christiaens D, Ades-Aron B, Sijbers J, Fieremans E. Denoising of diffusion MRI using random matrix theory. NeuroImage 2016;142:394–406.

13. Shamir RR, Duchin Y, Kim J, Sapiro G, Harel N. Continuous Dice Coefficient: a Method for Evaluating Probabilistic Segmentations. 2019. Available at: https://ui.adsabs.harvard.edu/abs/2019arXiv190611031S. Accessed October 10, 2022.

14. Wang Y, Wang Q, Haldar JP, Yeh FC, Xie M, Sun P, *et al.* Quantification of increased cellularity during inflammatory demyelination. Brain 2011;134:3590–601.

15. Slator PJ, Hutter J, Panagiotaki E, Rutherford MA, Hajnal JV, Alexander DC. IVIM MRI of the Placenta. In: Intravoxel Incoherent Motion (IVIM) MRI. Singapore: Jenny Stanford Publishing, 2018:317–338.

16. Barbu A, Ionasec R. Boosting cross-modality image registration. 2009. Available at: https://www.researchgate.net/publication/224545306_Boosting_cross-modality_image_registration. Accessed October 10, 2022.

17. Flouri D, Owen D, Aughwane R, Mufti N, Maksym K, Sokolska M, *et al.* Improved fetal blood oxygenation and placental estimated measurements of diffusion-weighted MRI using data-driven Bayesian modeling. Magn Reson Med 2020;83:2160–2172.

18. Le Bihan D, Poupon C, Amadon A, Lethimonnier F. Artifacts and pitfalls in diffusion MRI. J Magn Reson Imaging 2006;24:478–488.

19. Jones DK, Cercignani M. Twenty-five pitfalls in the analysis of diffusion MRI data. NMR Biomed 2010;23:803–820.

20. Fa-Hsuan L, Ying-Jui C, Belliveau JW, Wald LL. Removing signal intensity inhomogeneity from surface coil MRI using discrete wavelet transform and wavelet packet. 2001. Available at: https://www.researchgate.net/publication/224055305_Removing_signal_intensity_inhomogeneity_from_surface_coil_MRI_using_discrete_wavelet_transform_and_wavelet_packet. Accessed October 10, 2022.

21. Sørensen A, Hutter J, Seed M, Grant PE, Gowland P. T2*-weighted placental MRI: basic research tool or emerging clinical test for placental dysfunction? Ultrasound Obstet Gynecol 2020;55:293–302.

22. Ho AEP, Hutter J, Jackson LH, Seed PT, McCabe L, Al-Adnani M, *et al.* T2* placental magnetic resonance imaging in preterm preeclampsia: an observational cohort study. Hypertension 2020;75:1523–1531.

23. Otake Y, Kanazawa H, Takahashi H, Matsubara S, Sugimoto H. Magnetic resonance imaging of the human placental cotyledon: proposal of a novel cotyledon appearance score. Eur J Obstet Gynecol Reprod Biol 2019;232:82–86.

24. Mor G, Cardenas I, Abrahams V, Guller S. Inflammation and pregnancy: the role of the immune system at the implantation site. Ann N Y Acad Sci 2011;1221:80–87.

25. Ander SE, Diamond MS, Coyne CB. Immune responses at the maternal-fetal interface. Sci Immunol 2019;4:eaat6114.

26. Bonel HM, Stolz B, Diedrichsen L, Frei K, Saar B, Tutschek B, *et al.* Diffusion-weighted MR imaging of the placenta in fetuses with placental insufficiency. Radiology 2010;257:810–819.

27. Kingdom J, Huppertz B, Seaward G, Kaufmann P. Development of the placental villous tree and its consequences for fetal growth. Eur J Obstet Gynecol Reprod Biol 2000;92:35–43.

28. Turowski G, Vogel M. Re-view and view on maturation disorders in the placenta. APMIS 2018;126:602–612.

29. Wang Y, Zhao S. Vascular biology of the placenta. San Rafael (CA): Morgan & Claypool Life Sciences, 2010.

30. Slator PJ, Hutter J, McCabe L, Gomes ADS, Price AN, Panagiotaki E, *et al.* Placenta microstructure and microcirculation imaging with diffusion MRI. Magn Reson Med 2018;80:756–766.

31. Aughwane R, Ingram E, Johnstone ED, Salomon LJ, David AL, Melbourne A. Placental MRI and its application to fetal intervention. Prenat Diagn 2020;40:38–48.

32. Jakab A, Tuura R, Kottke R, Kellenberger CJ, Scheer I. Intra-voxel incoherent motion MRI of the living human foetus: technique and test-retest repeatability. Eur Radiol Exp 2017;1:26.

33. Aurioles-Garibay A, Hernandez-Andrade E, Romero R, Qureshi F, Ahn H, Jacques SM, *et al.* Prenatal diagnosis of a placental infarction hematoma associated with fetal growth restriction, preeclampsia and fetal death: clinicopathological correlation. Fetal Diagn Ther 2014;36:154–161.

34. Shi H, Quan X, Liang W, Li X, Ai B, Liu H. Evaluation of placental perfusion based on intravoxel incoherent motion diffusion weighted imaging (IVIM-DWI) and its predictive value for late-onset fetal growth restriction. Geburtshilfe Frauenheilkd 2019;79:396–401.